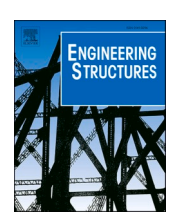
ELSEVIER

Contents lists available at ScienceDirect

Engineering Structures

journal homepage: www.elsevier.com/locate/engstruct





Behaviour and design of extended endplate hybrid steel beam-column connections at elevated temperatures

Chunyan Quan*, Luke Lapira , Katherine A. Cashell

Department of Civil Environmental and Geomatic Engineering, UCL, London, UK

ARTICLE INFO

Keywords:
Beam-column connections
Elevated temperatures
Finite element modelling
Fire
Stainless steel
Steel

ABSTRACT

In this paper, the behaviour of semi-rigid beam-column connections, with a primary focus on extended endplate connections, at ambient and elevated temperatures is investigated. Both pure carbon steel (including normal- and high-strength steel) connections and hybrid connections, i.e. incorporating carbon steel and stainless steel components, are considered. Upon validation against physical experiments, finite element models are developed to conduct comprehensive parametric studies, considering various combinations of endplate thicknesses and material grades, bolt sizes and material grades, and temperature levels. The numerical analyses results indicate that hybrid steel beam-column connections exhibit greater resistance and deformation capacity compared with carbon steel counterparts, especially at elevated temperatures greater than 500°C. The component-based design method provided in EN 1993–1–8:2024 for semi-rigid steel beam-column connections at ambient temperature is extended to cover fire scenarios; however, it only predicts the initial stiffness and plastic strength of beam-column connections. Therefore, another function is developed for predicting their ultimate strength at elevated temperatures. The developed fire design methods are shown to be safe and accurate through comparisons with the benchmark numerical results for carbon steel and hybrid steel and stainless steel beam-column connections.

1. Introduction

Previous studies have demonstrated that stainless steel beam-column connections offer greater strength and rotation capacity compared with geometrically identical carbon steel arrangements [1]. This advantage may be more significant under fire conditions, as stainless steel has superior elevated temperature material response than carbon steel [2]. Considering these benefits, while mitigating the high cost of using stainless steel throughout, this study proposes a hybrid steel beam-column connection, wherein carbon steel is replaced with stainless steel only in critical components, such as endplates and bolts.

Traditional design methods have predominantly focused on beam-column connections at ambient temperature, leaving a gap in the understanding of their behaviour during a fire. Therefore, in the current study, the behaviour of semi-rigid steel and hybrid steel beam-column connections, particularly extended endplate connections, at both ambient and elevated temperatures is investigated through numerical analysis. Key aspects such as initial stiffness, plastic strength, ultimate strength, deformation capacity and the bending moment-connection

rotation relationships are examined. In the comprehensive parametric studies, the influence of various parameters is analysed, including endplate thicknesses and material grades, bolt sizes and material grades, and temperature levels.

The European structural steel joint design standard EN 1993–1–8:2024 [3] provides the component-based method for design of steel beam-column connections. In the application of this design method, the beam-column connection is decomposed into several bolt-row springs and contact springs, which can be further decomposed into a series of individual active components. The mechanism behind this component-based design method is clear and straightforward, allowing for the prediction of initial stiffness and plastic strength [4]. However, its application has been limited to the design of connections at ambient temperature. Therefore, the current study aims to extend its application to also cover fire scenarios.

Owing to material strain hardening and stress redistribution, beamcolumn connections may exhibit non-negligible post-yielding stiffness and strength [4]. This effect may be more significant in the hybrid connections incorporating stainless steel components, owing to the

E-mail address: c.quan@ucl.ac.uk (C. Quan).

^{*} Corresponding author.

greater significance of material nonlinearity in the response of stainless steel to load, relative to carbon steel. The aforementioned component-based design method in EN 1993–1–8:2024 [3] currently only facilitates the prediction of initial stiffness and plastic strength, without considering post-yielding strength and stress redistribution. Therefore, in the current study, the approach proposed in [5] for the room temperature design of connections is extended to fire design, enabling the prediction of the bending moment-rotation curve up to the ultimate strength while considering the deformation capacity of the connections.

2. Finite element modelling

In the current study, solid finite element (FE) models are developed to simulate the behaviour of extended endplate beam-column connections at ambient and elevated temperatures. The development of the FE models is described in detail in this section, which are subsequently validated against experimental results from the literature.

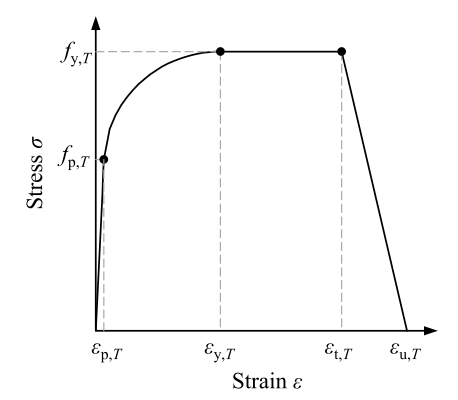
2.1. Development of finite element models

2.1.1. Modelling approach

The finite element analysis software ABAQUS [6] is utilised to carry out the numerical simulations. Isothermal analyses are conducted to investigate the behaviour of beam-column connections at elevated temperatures, where the temperature is uniformly increased in the simulation to a prescribed level, and then the load is applied to the structures while maintaining the constant elevated temperature. The STATIC, GENERAL solving procedure is employed in the FE modelling. The general purpose linear brick element with reduced integration C3D8R is implemented throughout the FE modelling, which has been successfully employed in previous relevant studies [7,8]. For contact interaction properties, hard contact is applied in the normal direction, while a penalty with a friction coefficient of 0.44 is used in the tangential direction, following the approach in [9]. To date, to the best of the authors' knowledge, there are few studies which accurately determine the friction coefficient between steel or stainless steel plates and bolts at elevated temperatures. Thus, the influence of elevated temperatures on the friction coefficient is not explored in the current study and will be considered in future work. To account for the effect of bolt fracture occurring in the threads regions, unthreaded round bar models with the reduced tensile stress area specified in ISO 3506-1 [10] are utilised for bolt modelling, as adopted in [11].

2.1.2. Material modelling

In the FE modelling, the four-stage material model provided in the $\,$



(a) Four-stage material model for carbon steel plates

European structural steel fire design standard EN 1993–1–2:2024 [12] is employed for carbon steel plates, as given by Eq. (1) and illustrated in Fig. 1(a).

$$\sigma = \begin{cases} \epsilon E_{T} & \text{for } \epsilon \leq \epsilon_{p,T} \\ f_{p,T} - c + (b/a)\sqrt{a^{2} - \left(\epsilon_{y,T} - \epsilon\right)^{2}} & \text{for } \epsilon_{p,T} < \epsilon < \epsilon_{y,T} \\ f_{y,T} & \text{for } \epsilon_{y,T} \leq \epsilon \leq \epsilon_{t,T} \\ f_{y,T} \left[1 - \left(\epsilon - \epsilon_{t,T}\right) \middle/ \left(\epsilon_{u,T} - \epsilon_{t,T}\right)\right] & \text{for } \epsilon_{t,T} < \epsilon < \epsilon_{u,T} \\ 0 & \text{for } \epsilon = \epsilon_{u,T} \end{cases}$$

$$(1)$$

In Eq. (1), σ and ε are the engineering stress and strain; E_T is the Young's modulus; $f_{p,T}$ and $f_{y,T}$ are the proportional limit stress and the stress at 2 % total strain; $\varepsilon_{p,T}$ and $\varepsilon_{y,T}$ are the strain at the proportional limit equal to $f_{p,T}/E_T$ and the 2 % total strain, respectively; $\varepsilon_{t,T}$ is the limit strain, currently set as 0.15; $\varepsilon_{u,T}$ is the ultimate strain equal to 0.20; and T is the elevated temperature to which the material is exposed, hence all parameters with a subscript T indicate that the parameter is evaluated at the elevated temperature indicated. The elevated temperature material properties E_T , $f_{p,T}$ and $f_{y,T}$ are determined by multiplying the room temperature material properties, i.e. the Young's modulus E and yield stress f_y , by the corresponding stiffness ($k_{E,T}$) and strength reduction factors ($k_{p,T}$, $k_{y,T}$) provided in EN 1993–1–2 [12], thus $E_T = k_E$, $f_{p,T} = k_{p,T}f_y$ and $f_{y,T} = k_{y,T}f_y$. The coefficients a, b and c are given as below as specified in EN 1993–1–2:2024 [12]:

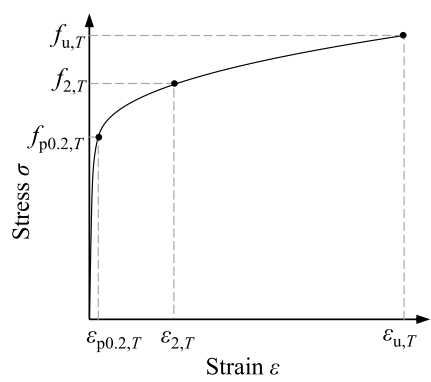
$$a = \sqrt{\left(\varepsilon_{y,T} - \varepsilon_{p,T}\right)\left(\varepsilon_{y,T} - \varepsilon_{p,T} + c/E_{T}\right)}$$
 (2)

$$b = \sqrt{c(\varepsilon_{y,T} - \varepsilon_{p,T})E_T + c^2}$$
(3)

$$c = \frac{\left(f_{y,T} - f_{p,T}\right)^2}{\left(\varepsilon_{y,T} - \varepsilon_{p,T}\right)E_T - 2\left(f_{y,T} - f_{p,T}\right)} \tag{4}$$

The two-stage Ramberg-Osgood material model. given in EN 1993–1–2:2024 [12], which has been verified for stainless steel [13] and bolts [14] at elevated temperatures, is utilised in the current study for modelling stainless steel plates and all bolts. The full stress-strain relationship is expressed by Eqs. (5) and (6) and illustrated in Fig. 1(b).

$$\varepsilon = \frac{\sigma}{E_T} + 0.002 \left(\frac{\sigma}{f_{\text{po.}2,T}}\right)^{n_T} \quad \text{for } \sigma \le f_{\text{po.}2,T}$$
 (5)



(b) Two-stage Ramberg-Osgood material model for stainless steel plates, high-strength steel plates and bolts

Fig. 1. Elevated temperature material models adopted in this study.

$$\mathrm{for} f_{\mathrm{p0.2,T}} < \sigma \leq f_{\mathrm{u,T}}$$

(6)

In Eqs. (5) and (6), $E_{p0.2,T}$ is the tangent modulus as given by Eq. (7):

$$E_{\text{p0.2,T}} = \frac{E_T}{1 + 0.002 n_T \frac{E_T}{f_{\text{n0.2,T}}}} \tag{7}$$

where $\varepsilon_{\text{p0.2,T}} = 0.002 + f_{\text{p0.2,T}} / E_T$ is the total strain at the 0.2 % proof stress $f_{\text{p0.2},T}$; $f_{\text{u},T}$ and $\varepsilon_{\text{u},T}$ are the ultimate strength and strain; and n_T and m_T are the strain hardening exponents. The elevated temperature material properties (i.e. E_T , $f_{p0.2,T}$, $f_{2,T}$, $f_{u,T}$, $\varepsilon_{u,T}$) are determined by multiplying the room temperature material properties, i.e. the Young's modulus E, yield (0.2 % proof) stress f_v , ultimate stress f_u and ultimate strain $\varepsilon_{\rm u}$, by the corresponding stiffness $(k_{\rm E.T})$, strength $(k_{\rm p0.2.T}, k_{\rm 2.T}, k_{\rm u.T})$ and ductility $(k_{eu,T})$ reduction factors provided in EN 1993-1-2:2024 [12] and Steel Construction Institute (SCI) Design Manual for Structural Stainless Steel [15], thus $E_T = k_{E,T}E$, $f_{p0.2,T} = k_{p0.2,T}f_y$, $f_{2,T} = k_{2,T}f_y$, $f_{u,T} = k_{2,T}f_y$, f $=k_{\mathrm{u},T}f_{\mathrm{u}}$ and $\varepsilon_{\mathrm{u},T}=k_{\varepsilon\mathrm{u},T}\varepsilon_{\mathrm{u}}$. In line with the recommendations in EN 1993–1–2:2024 [12], the first strain hardening exponent n_T , which defines the roundedness of the first stage of the elevated temperature material response, is taken equal to the room temperature value n. The second strain hardening exponent m_T , which defines the roundedness of the second stage of the elevated temperature material response, is calculated using Eq. (8) [12], thereby ensuring that the second stage of the two-stage Ramberg-Osgood material model passes through $f_{2,T}$ at 2 % total strain $\varepsilon_{2,T}$ and $f_{11,T}$ at the ultimate strain $\varepsilon_{11,T}$.

$$\ln \left(\frac{\frac{0.02 - \varepsilon_{p0.2,T} \cdot \frac{f_{2,T} - f_{p0.2,T}}{\varepsilon_{p0.2,T}}}{\varepsilon_{u,T} - \varepsilon_{p0.2,T} \cdot \frac{f_{u,T} - f_{p0.2,T}}{\varepsilon_{p0.2,T}}}}{\ln \left(\frac{f_{2,T} - f_{p0.2,T}}{f_{u,T} - f_{p0.2,T}} \right)} \right) \quad \text{but } 1.5 \le m_T \le 5$$
(8)

To investigate the behaviour of hybrid beam-column connections, end plates made from high strength steel S690 are also considered in the current study for comparison. The two-stage Ramberg-Osgood material model proposed in [16] is employed to model high strength steel at elevated temperatures, as given by Eqs. (5) and (9).

$$\varepsilon = \varepsilon_{\text{p0.2,T}} + \frac{\sigma - f_{\text{p0.2,T}}}{E_{\text{p0.2,T}}} + \varepsilon_{\text{u,T}} \left(\frac{\sigma - f_{\text{p0.2,T}}}{f_{\text{u,T}} - f_{\text{p0.2,T}}} \right)^{m_T} \text{ for } f_{\text{p0.2,T}} < \sigma \le f_{\text{u,T}}$$
 (9)

Note that Eq. (9), which represents the second stage of the high strength steel material model, is slightly different with Eq. (6), which is used for stainless steel. For high strength steel S690, the two strain hardening exponents proposed in [16] are taken as $n_T = 7$ -T/250 and $m_T = 1.6 + T/600$, where T is the temperature level. As required in ABAQUS [6], the aforementioned engineering stress-strain relationships should be converted into true stress-strain relationships. For data points before the necking point (the ultimate engineering stress point), i.e. when the true strain $\varepsilon_{\rm true}$ is not larger than the true strain at necking $\varepsilon_{\rm n}$, the true strain $\varepsilon_{\rm true}$ and true stress $\sigma_{\rm true}$ can be obtained using the following

equations

$$\varepsilon_{\text{true}} = \ln(1+\varepsilon)$$
 (10)

$$\sigma_{\text{true}} = \sigma(1 + \varepsilon) \quad \text{for } \varepsilon_{\text{true}} < \varepsilon_{\text{n}}$$
 (11)

Since component failure in FE analysis is determined by the material fracture strain, it is essential to include the descending stage after the necking point (i.e. the ultimate engineering stress point) in the engineering stress-strain curve for FE material data input. The relationship in Eq. (11) is derived under the assumption of uniaxial and uniform stress/strain. However, once necking begins, this assumption no longer holds due to highly localised deformations and triaxial stress states. To determine the exact true stress-strain relationship, accurate measurement of specimen geometry reduction is necessary, which is typically challenging to implement [11]. Therefore, in this study, following the approach in [17], the lower-bound post-necking true stress-strain relationship [18] is employed in the FE models. Hence, after the necking point, the true strain is still calculated using Eq. (10), while the true stress is determined as follows:

$$\sigma_{\rm true} = \sigma_{\rm n} (\varepsilon_{\rm true}/\varepsilon_{\rm n})^{\varepsilon_{\rm n}} \quad \text{for } \varepsilon_{\rm true} > \varepsilon_{\rm n}$$
 (12)

where σ_n represents the true stress at necking.

2.1.3. Failure criteria

Fracture is not explicitly modelled in the FE model, instead the criteria proposed in [19] are adopted to determine failure of connection components. Specifically: (i) bolt failure is identified when the average value of the principal strain at any cross-section of the bolt reaches the bolt material fracture strain, and (ii) plate component failure is determined by the principal strain value at any point attaining their respective material fracture strain. The true fracture strain of the material is obtained from isothermal tests and accounts only for mechanical strain without thermal strain. Thus, in the current study, the maximum principal logarithmic strain (i.e. LE_MAX_PRINCIPAL) is extracted from the numerical results to assess the component failure. Note that LE_MAX_-PRINCIPAL represents the true strain, not the engineering strain, and is the sum of thermal strain, elastic strain and plastic strain. Therefore, failure is evaluated by subtracting the thermal strain from the LE_MAX_PRINCIPAL value and checking the resulting mechanical strain against the true fracture strain of the material. Based on this strain assessment, the ultimate moment resistance and corresponding rotation capacity of the investigated beam-column connection at failure are established by considering the failure mode that occurs first during the loading procedure amongst the bending moment at: (i) bolt failure $M_{\rm u}$. bolt, (ii) plate failure $M_{u,plate}$, and (iii) the peak in the moment-rotation response $M_{u,max}$.

2.2. Validation of numerical models

The developed FE modelling approach is validated against the results from tests on high strength steel beam-column connections [7], including: (i) Q690 connections at ambient temperature labelled Q690A1 and Q690A2 (to confirm test repeatability), (ii) a Q690 connection at ambient temperature labelled Q960A1, (iii) a Q690 connection at 550°C labelled Q690F1, and (iv) Q960 connections at

Table 1Key material properties used in the FE models for validation studies.

Temperature	Steel grade	Yield strength (MPa)	Ultimate strength (MPa)	Elastic modulus (MPa)
Ambient temperature	Q690 [7]	763	796	198501
	Q960 [7]	1000	1040	200611
	Bolts 10.9 [20]	1085	1114	214500
550°C	Q690 [7]	423	444	108382
	Q960 [7]	631	646	106959
	Bolts 10.9 [20]	394	450	108855

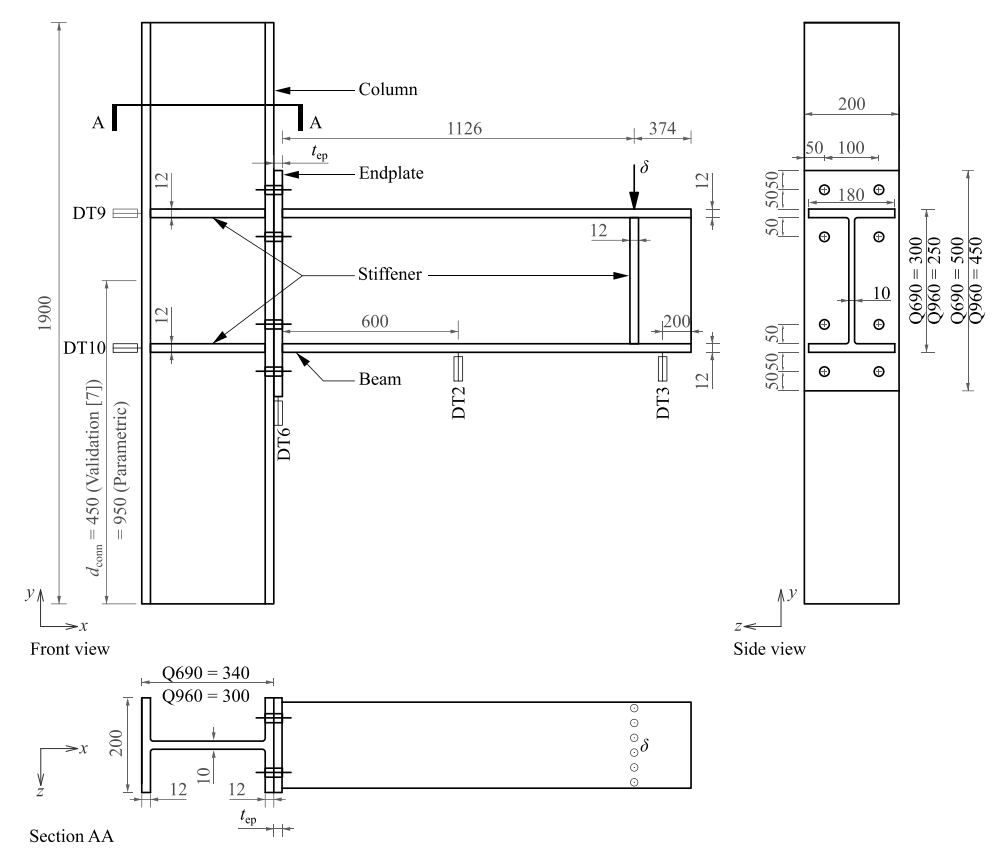


Fig. 2. Dimensions and location of displacement sensors for the specimens tested in [7] (all units are in mm).

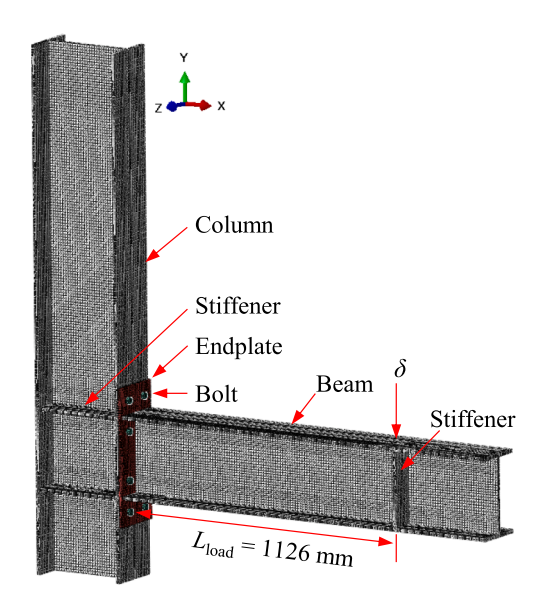


Fig. 3. FE model for validation study against tests conducted in [7].

550°C labelled Q960F1 and Q960F2 (also to confirm test repeatability). The material properties of high strength steel Q690 and Q960 as reported in [7] are employed in the FE models. In the absence of full stress-strain curves for G10.9 bolts [7], the material properties given in [20] are adopted herein. The key material properties adopted in the current FE models are listed in Table 1, while the geometric properties of

the FE models are identical to those reported in [7] and presented in Fig. 2. The dimensions of the column section, beam section and extended endplate are different for Q690 and Q960 connections. The endplate thickness $t_{\rm ep}$ of the tested specimens is 12 mm. The column height and beam length are 1900 mm and 1500 mm, respectively. In the validation study, the distance between the beam centreline and the bottom column end $d_{\rm conn}$ is 450 mm. A downwards displacement δ is applied at the stiffened cross-section near the beam end. The distance between the loading point and the endplate surface $L_{\rm load}$ is 1126 mm. Fixed boundary conditions are applied at top and bottom column ends. The developed FE model is presented in Fig. 3.

Fig. 4 presents the experimental and numerical bending moment-connection rotation M- θ curves of the tested connections in [7]. The bending moment M is calculated as the vertical load P, measured as the reaction force to the displacement δ applied at the beam end stiffener, multiplied by the distance L_{load} . The connection rotation θ is determined as follows,

$$\theta = \theta_{\rm b} - (\theta_{\rm c} + \gamma) \tag{13}$$

where θ_b and θ_c are the beam rotation and column rotation; γ is the shear deformation of the column web panel. The locations of displacement sensors on the specimens are illustrated in Fig. 2. Additional details on the ambient temperature tests can be found in [9]. For room temperature tests, the vertical displacements at DT2 and DT3, i.e. δ_{DT2} and δ_{DT3} , are employed to calculate θ_b , as given by:

$$\theta_{\rm b} = \arctan \frac{\left| \left(\delta_{\rm DT3} - \delta_{\rm b,el,DT3} \right) - \left(\delta_{\rm DT2} - \delta_{\rm b,el,DT2} \right) \right|}{700} \tag{14}$$

where $\delta_{\rm b,el,DTi}$ is the beam elastic displacement at the location of DTi, calculated by

$$\delta_{\text{b,el,DTi}} = -\frac{P}{E_{\text{b}}I_{\text{b}}} \left(\frac{x_{\text{DTi}}^{3}}{6} - \frac{L_{\text{load}}x_{\text{DTi}}^{2}}{2} \right)$$
 (15)

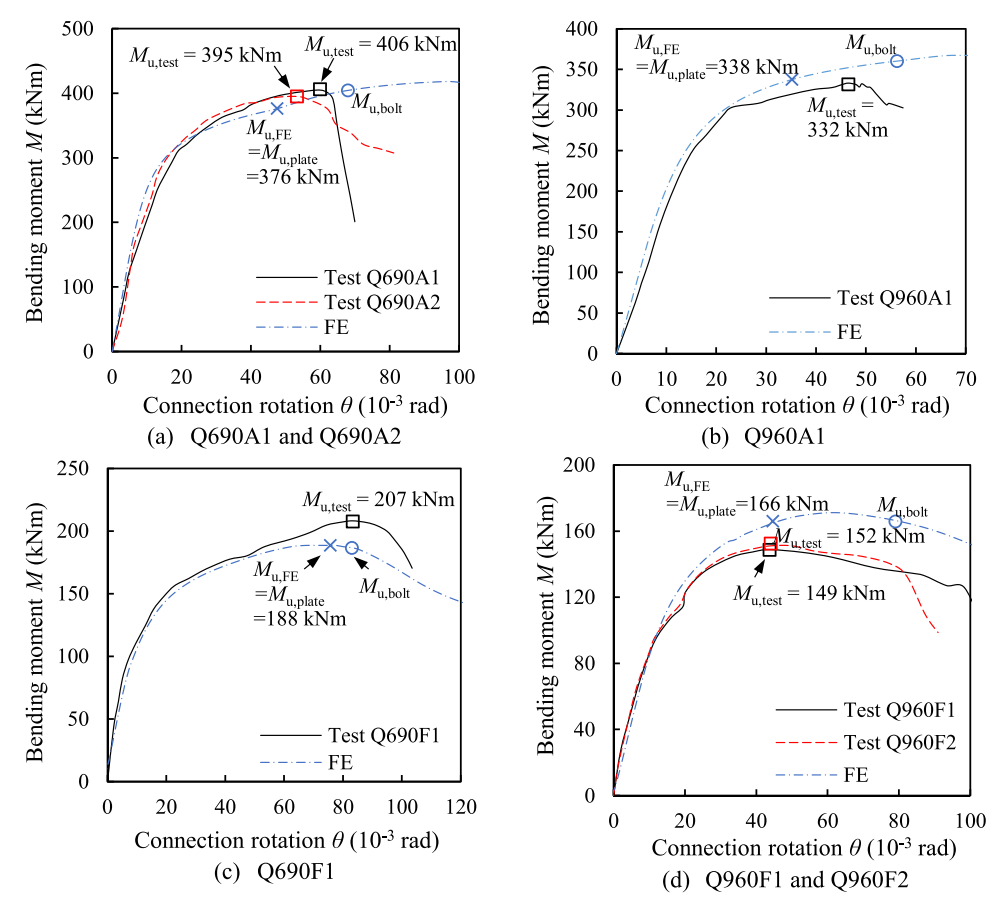


Fig. 4. Comparison of experimental and numerical M- θ curves of beam-column connections tested in [7].

and x_{DTi} is the distance from DTi to the endplate surface.

For elevated temperature tests, the vertical displacements at DT2 and DT6, i.e. δ_{DT2} and δ_{DT6} , are used to calculate θ_b as described in [7]:

$$\theta_{\rm b} = \arctan \frac{\left| \left(\delta_{\rm DT2} - \delta_{\rm b,el,DT2} \right) - \delta_{\rm DT6} \right|}{600} \tag{16}$$

The column rotation θ_c and the shear deformation of the column web panel γ used in Eq. (13) are calculated as follows:

$$\theta_{\rm c} + \gamma = \arctan \frac{|\delta_{\rm DT9} - \delta_{\rm DT10}|}{h_{\rm b} - t_{\rm fb}} \tag{17}$$

where $\delta_{\rm DT9}$ and $\delta_{\rm DT10}$ are the horizontal displacements at the column points DT9 and DT10, and $h_{\rm b}$ and $t_{\rm fb}$ are the beam depth and beam flange thickness, respectively.

In addition to the M- θ curves, the experimental ultimate strength $M_{\rm u}$. test, bending moment at bolt failure $M_{\text{u,bolt}}$ and at plate failure $M_{\text{u,plate}}$ from the FE analysis are also indicated in Fig. 4. In the FE analysis of these specimens, the bolt failure occurs shortly after the endplate failure, thus it is assumed that the failure and ultimate strength $M_{\rm u.FE}$ of the connections is dominated by the endplate; this is also consistent with the reported test observations of endplate yielding with severe deformation and bolt fracture in [7]. It is seen in Fig. 4 that the numerical bending moment-rotation curves closely align with the test curves up to the experimental ultimate strength $M_{u,test}$, and then deviate beyond that point. This deviation is primarily attributed to the fact that, to mitigate convergence issues and enhance model reliability, fracture is not explicitly modelled in the FE models. Instead, the lower-bound post-necking true stress-strain relationship [18] is employed in conjunction with the failure criteria proposed elsewhere [19] to determine failure of connection components (see Section 2.1.3). While this approach may not fully capture the load redistribution that occurs following initial

component fracture, which leads to the declining trend in the experimental responses, it consistently yields resistances and failure modes that are in good agreement with the test results, demonstrating its effectiveness. The experimental and numerical ultimate strengths, $M_{\rm u}$ test and $M_{\rm u.FE}$, and experimental and numerical initial stiffnesses, $K_{\rm ini.test}$ and $K_{\text{ini,FE}}$, as well as the ratio of numerical results to experimental results are presented in Table 2. The maximum discrepancy between the numerical and experimental ultimate strengths is within 12 %, indicating the accuracy of the developed FE models. Meanwhile, the initial stiffness of the numerical results compares reasonably well with the experimental results for room temperature tests but are conservative for elevated temperature tests. A qualitative comparison between the experimental and numerical failure modes of the beam-column connections tested in [7] is presented in Fig. 5, where the latter also depicts the distribution of maximum principal logarithmic strain at the failure moment. The numerical results show good consistency with the experimental observations.

3. Parametric studies and fire behaviour of connections

Following validation, the developed FE models are then employed to conduct extensive parametric studies, investigating the effects of various parameters on the connection behaviour.

3.1. Parametric studies

The configuration and geometry properties of each component in the beam-column connections for parametric studies are the same as those in the Q690 connections tested in [7], as shown in Fig. 2, except for the beam centreline which is shifted upwards to align with the column mid-height, i.e. d_{conn} equal to half the column length 950 mm. This is

 Table 2

 Comparison of numerical ultimate connection capacities and initial stiffnesses against the experimental results reported in [7].

Test ID	Temperature	$M_{\rm u,test}$ (kNm)	$M_{\rm u,FE}$ (kNm)	$M_{\rm u,FE}/M_{\rm u,test}$	$K_{\text{ini,test}}$ (kNm/rad)	$K_{\text{ini,FE}}$ (kNm/rad)	$K_{\rm ini,FE}/K_{\rm ini,test}$
Q690A1	Ambient temperature	406.32	376.44	0.93	26271	26009	0.99
Q690A2		394.98	376.44	0.95	26297	26009	0.99
Q960A1		331.67	337.57	1.02	17363	18802	1.08
Q690F1	550°C	207.39	188.43	0.91	17434	11776	0.68
Q960F1		148.73	165.85	1.12	11478	8911	0.78
Q960F2		152.44	165.85	1.09	10427	8911	0.85

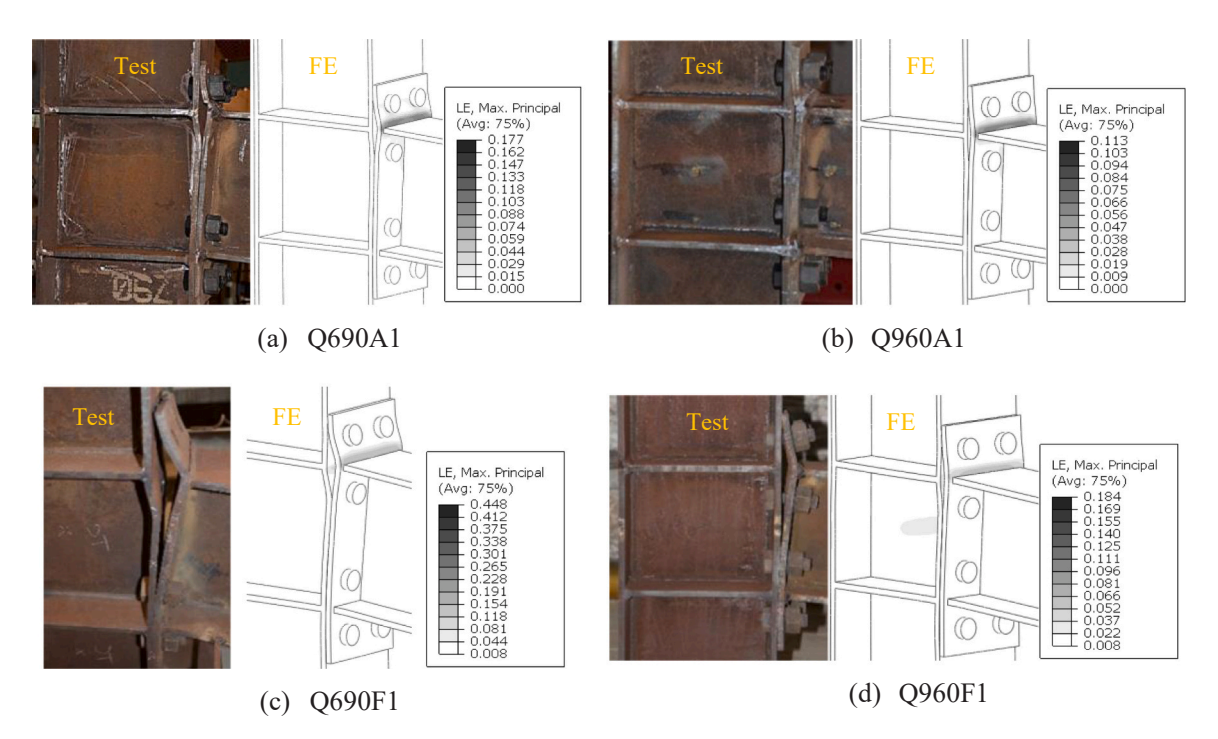


Fig. 5. Comparison of experimental and numerical failure modes of beam-column connections tested in [7].

done to reduce the influence of the column boundary conditions on the connection response. The column height and beam length are 1900 mm and 1500 mm, respectively. The distance between the endplate surface and the loading point is 1126 mm, and a downwards displacement is applied. The bottom end of the column is fixed, and the top end is restrained in rotation but allowed to expand freely in the longitudinal direction.

In all cases, the beam, column and stiffeners are made of carbon steel S355. As summarised in Table 3, the beam-column connection with an endplate made from S355 with a thickness of 12 mm and G8.8 bolts of

Table 3Summary of parametric studies on steel and hybrid beam-column connections.

No.	Endplate material	Endplate thickness (mm)	Bolt material	Bolt size	Temperature (°C)
1	S355	12	G8.8	M20	20, 300, 500,
2	S690	12	G8.8	M20	700
3	A1.4420	12	G8.8	M20	
4	D1.4410	12	G8.8	M20	
5	F1.4509	12	G8.8	M20	
6	S355	12	G10.9	M20	
7	S355	12	A4-70	M20	
8	A1.4420	12	A4-70	M20	
9	D1.4410	12	A4-70	M20	
10	F1.4509	12	A4-70	M20	
11	S355	10	G8.8	M20	
12	S355	15	G8.8	M20	
13	S355	12	G8.8	M16	
14	S355	12	G8.8	M24	

size M20 is taken as the benchmark case. In order to investigate the influence of various parameters including endplate material grade, bolt material grade, endplate thickness and bolt size on the behaviour of steel and hybrid endplate beam-column connections at different temperature levels, with consideration of both endplate and bolt failure modes, the following model parameters are varied in the current study: (i) the endplate material grade between S355, S690, austenitic stainless steel 1.4420 (A1.4420), duplex stainless steel 1.4410 (D1.4410) and ferritic stainless steel 1.4509 (F1.4509), respectively denoted as S355/S690/ A420/D410/F509 in the specimen labels as given in Table 4; (ii) the bolt material grade between G8.8, G10.9 and stainless steel A4-70, respectively denoted as B8/B10/BA47; (iii) the endplate thickness of 10, 12 and 15 mm, respectively denoted as E10/E12/E15; (iv) the bolt size of M16, M20 and M24 and (v) the temperature levels of 20°C, 300°C, 500°C and 700°C, respectively given as R/T300/T500/T700. The specimens are named in the format: "endplate material-endplate thickness-bolt material-bolt size-temperature level". For example, the benchmark case at room temperature is named as S355-E12-B8-M20-R. The elevated temperature material models described in Section 2.1.2 are employed in the FE models. The utilised stiffness, strength and ductility material properties are taken as those values provided in [12] for carbon steel grade S355, [21] for high strength steel grade S690, [22] for austenitic stainless steel grade 1.4420, [23] for duplex stainless steel grade 1.4410, [24] for ferritic stainless steel grade 1.4509, [20] for the G8.8/G10.9 bolts and [25] for stainless steel grade A4-70 bolts.

The initial stiffness $K_{\text{ini,FE}}$, plastic resistance $M_{\text{y,FE}}$ and ultimate resistance $M_{\text{u,FE}}$ obtained from FE models for all studied beam-column connections at different temperature levels are listed in Tables 4–7.

The bending moment-rotation M- θ curves for the studied connections are presented in Figs. 6–11. The approach used to derive the M- θ curves is the same as that adopted in the validation studies for elevated temperature tests, i.e. employing the displacements at DT2 and DT6 to calculate the beam rotation θ_b and the displacements at DT9 and DT10 to calculate the column rotation and shear deformation of column web panel θ_c + γ .

3.2. Fire behaviour of connections

3.2.1. Bolt size

As summarised in Table 3, the connections with bolt sizes of M16, M20 and M24 are considered in the current study. Fig. 6 presents the

bending moment-rotation (M- θ) curves for steel beam-column connections with different bolt sizes at room temperature (20°C) and elevated temperatures 300°C, 500°C and 700°C. The ultimate connection resistances are also indicated in the figure. At 20°C and 300°C, the beam-column connection with the M20 bolt size (i.e. the benchmark case) fails when the plate strain reaches its fracture strain, thus the numerical connection resistance $M_{\rm u,FE}$ is taken as $M_{\rm u,plate}$. For these cases, increasing the bolt size to M24 postpones the bolt failure and enhances the connection resistance, however, slightly reduces the rotation at the ultimate resistance. This is attributed to fact that the larger bolt is stiffer, resulting in reduced load redistribution to the plate. Conversely, at 20°C and 300°C, reducing the bolt size to M16 renders the bolt as the weakest element in the connection, and hence the failure mode shifts from plate

Table 4Numerical and predicted initial stiffness, plastic resistance and ultimate resistance of beam-column connections at room temperature.

Name	K _{ini,FE} (kNm/rad)	M _{y,FE} (kNm)	M _{u,FE} (kNm)	K _{ini,pre} (kNm/rad)	M _{y,pre} (kNm)	M _{u,pre} (kNm)	$K_{ m ini,pre}/$ $K_{ m ini,FE}$	$M_{ m y,pre}/$ $M_{ m y,FE}$	$M_{ m u,pre}/$ $M_{ m u,FE}$
S355-E12-B8-M20-R	22680	130.5	181.3	19773	116.4	136.2	0.87	0.89	0.75
S355-E12-BA47-M20-R	22256	133.2	180.2	19663	117.1	136.8	0.88	0.88	0.76
A420-E12-B8-M20-R	23215	136.6	200.2	20233	116.7	151.5	0.87	0.85	0.76
D410-E12-B8-M20-R	21542	163.4	213.2	18985	146.9	176.1	0.88	0.90	0.83
F509-E12-B8-M20-R	22919	135.5	194.6	20014	117.8	144.4	0.87	0.87	0.74
A420-E12-BA47-M20-R	22860	139.9	206.1	20118	117.5	152.1	0.88	0.84	0.74
D410-E12-BA47-M20-R	21293	168.0	214.7	18881	147.6	176.6	0.89	0.88	0.82
F509-E12-BA47-M20-R	22570	138.5	203.8	19902	118.5	145.0	0.88	0.86	0.71
S355-E12-B8-M24-R	25162	145.1	199.2	20024	134.3	154.2	0.80	0.93	0.77
S355-E12-B8-M16-R	20216	113.5	130.3	19379	94.6	114.0	0.96	0.83	0.87
S355-E12-B10-M20-R	22719	135.8	181.1	19785	129.1	148.8	0.87	0.95	0.82
S690-E12-B8-M20-R	22152	166.6	214.6	19437	161.1	180.1	0.88	0.97	0.84
S355-E15-B8-M20-R	26950	154.0	203.4	23404	138.8	162.2	0.87	0.90	0.80
S355-E10-B8-M20-R	18790	100.7	149.0	16404	90.5	106.9	0.87	0.90	0.72

Table 5Numerical and predicted initial stiffness, plastic resistance and ultimate resistance of beam-column connections at 300°C.

Name	K _{ini,FE} (kNm/rad)	M _{y,FE} (kNm)	M _{u,FE} (kNm)	K _{ini,pre} (kNm/rad)	M _{y,pre} (kNm)	M _{u,pre} (kNm)	$K_{\rm ini,pre}/$ $K_{\rm ini,FE}$	$M_{ m y,pre}/$ $M_{ m y,FE}$	$M_{ m u,pre}/$ $M_{ m u,FE}$
S355-E12-B8-M20-T300	18670	114.4	179.4	15944	121.4	137.1	0.85	1.06	0.76
S355-E12-BA47-M20-T300	17960	113.0	159.0	15776	106.1	121.8	0.88	0.94	0.77
A420-E12-B8-M20-T300	15611	97.2	205.7	13400	101.2	124.4	0.86	1.04	0.60
D410-E12-B8-M20-T300	19018	141.0	205.9	15743	144.8	167.4	0.83	1.03	0.81
F509-E12-B8-M20-T300	20014	110.9	197.9	16966	115.8	140.7	0.85	1.04	0.71
A420-E12-BA47-M20-T300	14777	98.0	161.2	13273	93.0	116.0	0.90	0.95	0.72
D410-E12-BA47-M20-T300	17764	140.2	174.6	15579	129.6	152.0	0.88	0.92	0.87
F509-E12-BA47-M20-T300	19347	110.7	161.7	16780	101.8	126.4	0.87	0.92	0.78
S355-E12-B8-M24-T300	20847	127.9	195.2	16112	134.3	150.0	0.77	1.05	0.77
S355-E12-B8-M16-T300	16677	101.4	143.7	15677	97.8	113.4	0.94	0.96	0.79
S355-E12-B10-M20-T300	18680	119.7	178.5	15953	129.0	144.6	0.85	1.08	0.81
S690-E12-B8-M20-T300	19672	150.8	212.8	16739	164.2	154.9	0.85	1.09	0.73
S355-E15-B8-M20-T300	22242	137.1	201.9	18906	143.8	162.5	0.85	1.05	0.80
S355-E10-B8-M20-T300	15501	90.3	149.8	13211	90.5	103.6	0.85	1.00	0.69

Table 6
Numerical and predicted initial stiffness, plastic resistance and ultimate resistance of beam-column connections at 500°C.

Name	K _{ini,FE} (kNm/rad)	M _{y,FE} (kNm)	M _{u,FE} (kNm)	K _{ini,pre} (kNm/rad)	M _{y,pre} (kNm)	M _{u,pre} (kNm)	$K_{ m ini,pre}/$ $K_{ m ini,FE}$	$M_{ m y,pre}/$ $M_{ m y,FE}$	$M_{ m u,pre}/M_{ m u,FE}$
S355-E12-B8-M20-T500	14294	80.5	102.6	12004	74.8	86.8	0.84	0.93	0.85
S355-E12-BA47-M20-T500	13190	84.9	134.9	11940	89.7	101.5	0.91	1.06	0.75
A420-E12-B8-M20-T500	13127	75.7	103.4	10685	69.9	88.3	0.81	0.92	0.85
D410-E12-B8-M20-T500	15387	100.4	113.0	12520	89.5	80.1	0.81	0.89	0.71
F509-E12-B8-M20-T500	16434	82.6	104.1	13612	76.8	88.5	0.83	0.93	0.85
A420-E12-BA47-M20-T500	12177	81.9	147.2	10632	84.7	103.0	0.87	1.03	0.70
D410-E12-BA47-M20-T500	14618	110.6	162.0	12452	115.8	128.9	0.85	1.05	0.80
F509-E12-BA47-M20-T500	16146	87.5	145.2	13533	91.6	103.1	0.84	1.05	0.71
S355-E12-B8-M24-T500	15894	91.5	137.1	12118	88.6	100.6	0.76	0.97	0.73
S355-E12-B8-M16-T500	12790	66.8	71.4	11822	61.4	60.4	0.92	0.92	0.85
S355-E12-B10-M20-T500	14023	86.5	138.9	11933	88.6	100.4	0.85	1.02	0.72
S690-E12-B8-M20-T500	15815	103.9	115.2	13172	90.4	82.0	0.83	0.87	0.71
S355-E15-B8-M20-T500	16987	94.3	111.1	14247	87.6	82.3	0.84	0.93	0.74
S355-E10-B8-M20-T500	11828	65.2	97.2	9941	60.9	70.8	0.84	0.93	0.73

Table 7Numerical and predicted initial stiffness, plastic resistance and ultimate resistance of beam-column connections at 700°C.

Name	K _{ini,FE} (kNm/rad)	M _{y,FE} (kNm)	M _{u,FE} (kNm)	K _{ini,pre} (kNm/rad)	M _{y,pre} (kNm)	M _{u,pre} (kNm)	$K_{ m ini,pre}/$ $K_{ m ini,FE}$	$M_{ m y,pre}/M_{ m y,FE}$	$M_{ m u,pre}/M_{ m u,FE}$
S355-E12-B8-M20-T700	3308	23.9	25.6	2624	20.1	22.7	0.79	0.84	0.88
S355-E12-BA47-M20-T700	3439	30.3	48.2	2668	30.0	32.3	0.78	0.99	0.67
A420-E12-B8-M20-T700	4619	28.3	30.2	3577	23.7	22.7	0.77	0.84	0.75
D410-E12-B8-M20-T700	4904	30.2	31.4	3550	24.3	23.1	0.72	0.80	0.73
F509-E12-B8-M20-T700	4631	26.7	28.6	3495	23.1	22.2	0.75	0.86	0.77
A420-E12-BA47-M20-T700	4581	43.9	60.7	3658	44.7	48.7	0.80	1.02	0.80
D410-E12-BA47-M20-T700	4536	47.4	63.7	3629	47.3	49.8	0.80	1.00	0.78
F509-E12-BA47-M20-T700	5077	41.5	59.3	3571	42.0	39.3	0.70	1.01	0.66
S355-E12-B8-M24-T700	3716	28.9	34.3	2643	23.2	25.8	0.71	0.80	0.75
S355-E12-B8-M16-T700	2969	16.8	17.7	2593	13.7	13.9	0.87	0.81	0.78
S355-E12-B10-M20-T700	3177	21.7	23.3	2591	18.5	19.7	0.82	0.85	0.85
S690-E12-B8-M20-T700	4486	25.1	26.6	3378	20.7	20.3	0.75	0.83	0.76
S355-E15-B8-M20-T700	3939	26.0	27.1	3120	21.5	20.5	0.79	0.83	0.75
S355-E10-B8-M20-T700	2774	21.0	23.9	2170	15.9	18.1	0.78	0.76	0.76

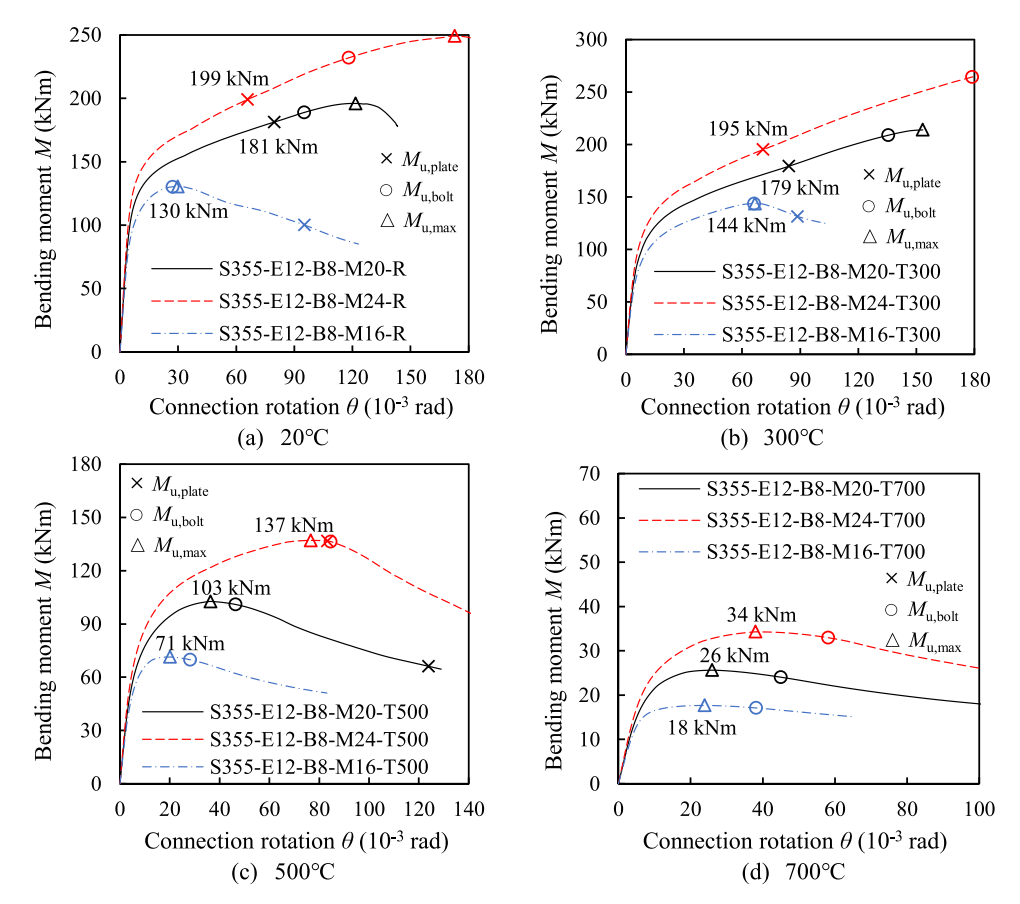


Fig. 6. M- θ curves of connections incorporating Grade 8.8 carbon steel bolts of various sizes at temperatures of (a) 20°C, (b) 300°C, (c) 500°C and (d) 700°C.

failure to bolt failure, thus the numerical connection resistance $M_{\rm u,FE}$ is taken as $M_{\rm u,bolt}$. This reduction in bolt size also results in a reduction of both the ultimate resistance and the rotation at the ultimate resistance. It is noted in Fig. 6(a) and (b) that the connection with M16 bolts exhibits higher ultimate resistance at 300°C (144 kNm) compared to the corresponding resistance at room temperature (130 kNm). This is most likely owing to the material properties of the G8.8 bolts used in the current study, as provided by [20], which indicate a higher ultimate strength $f_{\rm u,T}=940$ MPa at 300°C than the room temperature value $f_{\rm u}=865$ MPa.

At 500°C and 700°C, all of the beam-column connections with Grade 8.8 bolts of diameter M16, M20 or M24 fail due to the maximum bending moment reached followed by bolt failure; hence, increasing the bolt size enhances both the ultimate connection resistance and the

rotation at the ultimate resistance. In addition to ultimate resistances, Tables 4–7 also provide comparisons of initial stiffness and plastic strength (see details in Section 5) for beam-column connections with various bolt sizes. It is further observed that at both ambient temperature and elevated temperatures, the initial stiffness and plastic strength of the connections also increase with larger bolt diameter.

3.2.2. Endplate thickness

Various endplate thicknesses (10, 12 and 15 mm) made from S355 carbon steel are also considered in the parametric studies. The bending moment-rotation (M- θ) curves of connections with various endplate thicknesses at different temperature levels are presented in Fig. 7. It can be seen that at 20°C and 300°C, the connections exhibit endplate failure, whereas at 500°C and 700°C, the failure mode is dominated by the peak

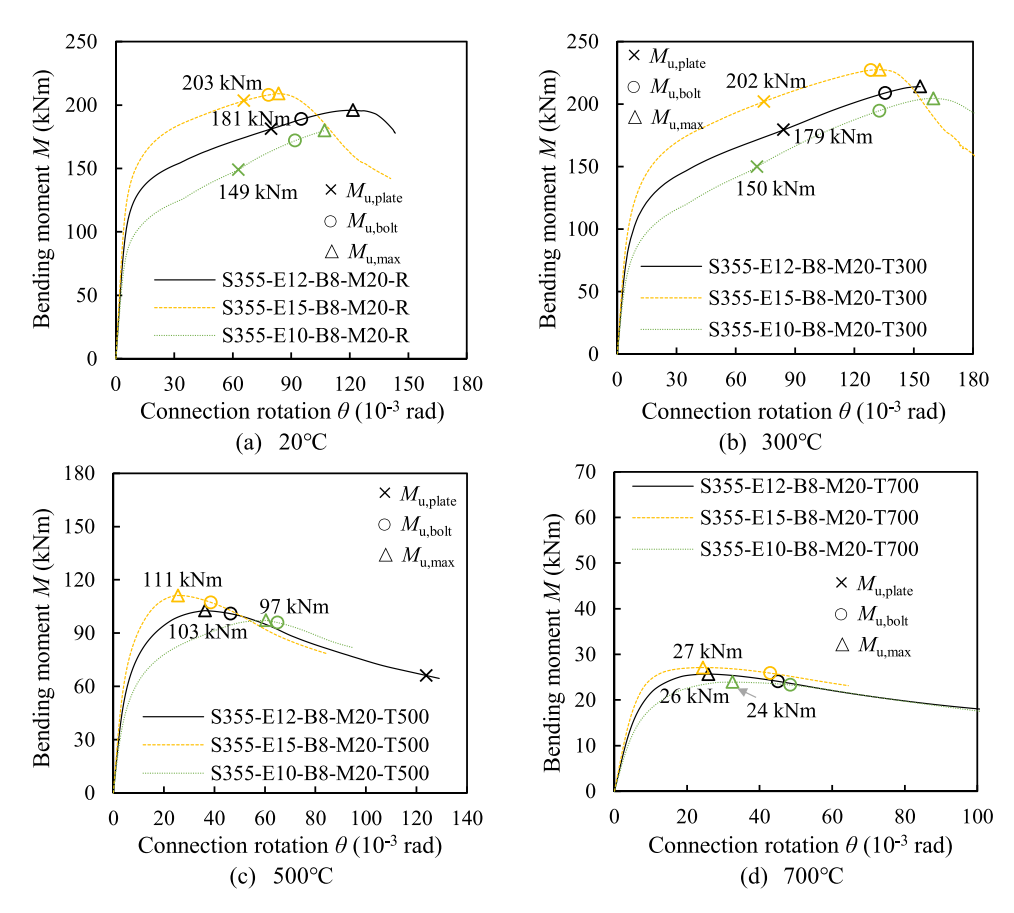


Fig. 7. M-θ curves of connections incorporating S355 endplates with various thicknesses at temperatures of (a) 20°C, (b) 300°C, (c) 500°C and (d) 700°C.

bending moment reached in the M- θ response. At all temperature levels, increasing the endplate thickness resulted in higher ultimate resistance. As shown in Tables 4–7, the initial stiffness and plastic strength of the connections also increase with increasing endplate thickness.

3.2.3. Bolt material grade

In addition to the commonly used G8.8 and G10.9 bolts, bolts made of stainless steel A4-70 are also considered in the current study. Fig. 8 presents the bending moment-rotation $M-\theta$ curves for connections incorporating M20 bolts made of various material grades. At ambient temperature, all three connections fail due to endplate failure; thus, changing the bolt material grade has minimal effect on the ultimate connection resistance. At 300°C, replacing G8.8 bolts with G10.9 bolts results in the connection still failing due to endplate failure, with no change in the ultimate connection resistance, yet resulting in a 17 % reduction in the rotational capacity of the connection owing to the reduced ductility of the G10.9 bolts. However, replacing the G8.8 bolts with stainless steel A4-70 bolts results in a shift in the failure mode from endplate failure to bolt failure, which reduces the ultimate connection resistance by 11 %. Although the stainless steel A4-70 bolts [25] have similar room temperature properties (e.g. $f_{\rm y}=676\,{\rm MPa}$ and $f_{\rm u}=$ 876 MPa) to the G8.8 bolts [20] (e.g. $f_y = 668$ MPa and $f_u = 865$ MPa), the stainless steel A4-70 bolts [25] exhibit significantly lower ultimate strength at 300°C ($f_{u,T} = 711$ MPa) compared to the G8.8 bolts ($f_{u,T} =$ 940 MPa). Additionally, it is important to recall that the ultimate strength of G8.8 bolts at 300°C is higher than its room temperature strength. However, at higher elevated temperatures, e.g. 500°C and 700°C, the hybrid beam-column connections with stainless steel A4-70 bolts demonstrate significantly greater ultimate resistance and rotation capacity compared to the counterparts with G8.8 bolts, as shown in Fig. 8(c) and (d), owing to the superior elevated temperature stiffness and strength retention ability of stainless steel.

3.2.4. Endplate material grade

The behaviour of connections incorporating 12 mm thick endplates made of carbon steel S355, high strength steel S690, grade 1.4420 austenitic stainless steel, grade 1.4410 duplex stainless steel and grade 1.4509 ferritic stainless steel is investigated in the current section, and the bending moment-rotation M- θ responses are presented in Fig. 9. At 20°C and 300°C, replacing the S355 endplate with S690 or stainless steel endplates improves the ultimate connection resistance, owing to their higher resistances compared with S355. Additionally, grade 1.4420 austenitic stainless steel and grade 1.4509 ferritic stainless steel endplates are also beneficial for improving the connection rotation capacity, owing to their improved material ductility. At 500°C and 700°C, all connections failed when the peak bending moment is reached; thus, while replacing the S355 endplate with stainless steel endplates does improve the ultimate connection resistance, the gains are marginal.

3.2.5. Bolt and endplate material grade

Fig. 10 presents the bending moment-rotation M- θ curves for the benchmark carbon steel connection compared with hybrid connections that incorporate stainless steel in both the endplates and the bolts. As shown in Fig. 10 (b) for the response at 300°C, the carbon steel connection demonstrates a higher ultimate connection resistance compared with the hybrid connections incorporating stainless steel endplates and bolts. This is attributed to the fact that the G8.8 bolts have an ultimate strength higher than that of stainless steel A4–70 bolts [25] and even surpass their own ultimate strength at room temperature, as described in Section 3.2.3. However, at other temperature levels, replacing carbon steel endplates and bolts with stainless steel components leads to higher ultimate connection resistances. This is particularly evident at 500°C and 700°C, as shown in Fig. 10 (c)-(d), owing to the superior ductility of stainless steel at higher elevated temperatures, the ultimate resistances and rotation capacities of the hybrid connections

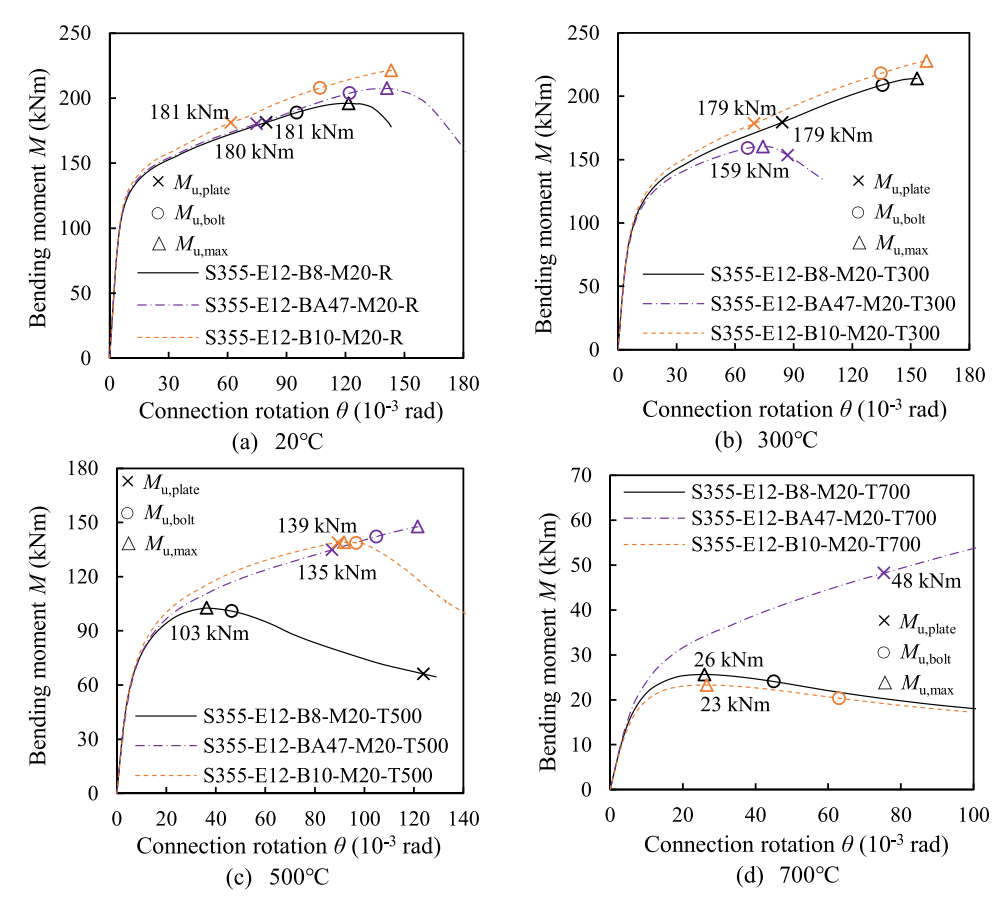


Fig. 8. M-θ curves of connections incorporating M20 bolts made of various material grades at temperatures of (a) 20°C, (b) 300°C, (c) 500°C and (d) 700°C.

are also significantly improved, highlighting the advantages of hybrid connections for fire-resistant design.

3.2.6. Boundary conditions

In addition to considering the influence of various bolt and endplate sizes and material grades, the effect of boundary conditions at the top end of the column is also considered herein. Fig. 11 presents the moment-rotation $M-\theta$ curves for the connection S355-E12-B8-M16-T700 with different boundary conditions at the top end of the column, where: (A) corresponds to unrestrained thus the column is allowed to expand freely with increasing temperature, (B) refers to a fixed connection during both heating and loading steps, thereby restraining thermal expansion, and (C) means that the connection is fixed only during the loading step, thereby allowing thermal expansion during the heating process. The numerical initial stiffnesses of connections with three boundary conditions, denoted as Kini, FE, A, Kini, FE, B and Kini, FE, C, respectively, and the corresponding ultimate connection strengths, denoted as $M_{\text{u.FE.A}}$, $M_{\text{u.FE.B}}$ and $M_{\text{u.FE.C}}$, respectively, are also shown in the figure. It is observed that $M_{u,FE,A}$, $M_{u,FE,B}$ and $M_{u,FE,C}$ are almost identical, indicating that if the top end of the column is fixed - whether during both heating and loading steps or only during the loading step - it has minimal influence on the ultimate connection strength. However, $K_{\text{ini,FE,B}}$ is significantly lower than $K_{\text{ini},\text{FE},A}$, showing that the thermal forces or stresses existing in the column resulting from the axial restraints caused by the fixed boundary conditions greatly reduce the initial stiffness. This reduction in stiffness is a result of thermal effects, since the connection with condition C, i.e. where the boundary condition is only fixed during the loading step, exhibits similar results to condition A, i.e. where the column is allowed to freely expand throughout. Since the componentbased design method in EN 1993-1-8 [3] is intended for the design of joints at ambient temperature, these thermal effects are not taken into account. Similarly, the design proposals which are presented in Section

4, are applicable only to connections where the columns are free to expand. Hence, for design cases where the columns are fixed during the heating process, the stiffness predictions may be unsuitable. A comprehensive investigation into the influence of thermal forces caused by restrained column or beam boundary conditions will be undertaken in future research, outside of the scope of the current paper.

4. Design methodologies for hybrid connections in fire

The European structural steel design standard EN 1993–1–8:2024 [3] provides a component-based method for room temperature design of steel beam-column connections, enabling the prediction of the initial stiffness and plastic resistance. In this design method, the beam-column connection is decomposed into several bolt-row springs and contact springs, which can be further decomposed into a series of individual active components, as shown in Fig. 12 (a) and (b). For the studied extended endplate beam-column connections, the active components include: (i) tension zone: column web in tension, column flange in bending, endplate in bending, beam web in tension, bolts in tension; (ii) compression zone: column web in compression, beam flange and web in compression and (iii) shear zone: column web panel in shear.

4.1. Initial stiffness

According to EN 1993–1–8:2024 [3], the initial stiffness of the beam-column connection is calculated by treating individual component elements as separate springs. In the current study, the spring model given in EN 1993–1–8:2024 [3] for room temperature design is adapted for elevated temperature scenarios by taking into account the degradation of material stiffness, i.e. the elevated temperature material stiffness is used in place of room temperature stiffness in the EN 1993–1–8:2024 [3] formulations. Thus, the initial stiffness $K_{\rm ini}$ of the

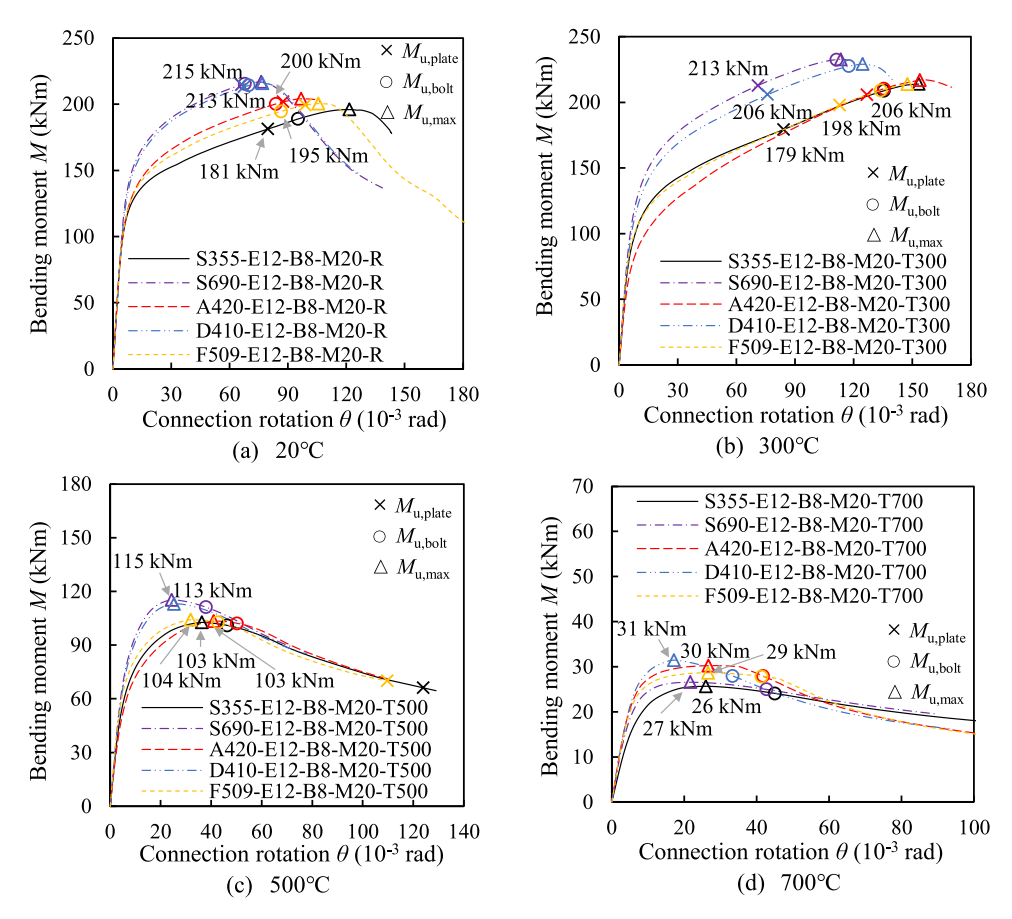


Fig. 9. M-θ curves of connections incorporating 12 mm thick endplates made of various material grades at temperatures of (a) 20°C, (b) 300°C, (c) 500°C and (d) 700°C.

extended endplate beam-column connection can be predicted as follows:

$$K_{\rm ini} = \frac{z_{\rm eq}^2}{\frac{1}{k_{\rm eq}} + \frac{1}{k_{\rm c}} + \frac{1}{k_{\rm v}}} \tag{18}$$

In Eq. (18), z_{eq} is the equivalent lever arm given by

$$z_{\text{eq}} = \frac{\sum_{i} k_{\text{eff,i}} h_{i}^{2}}{\sum_{i} k_{\text{eff,i}} h_{i}}$$

$$\tag{19}$$

where:

- i represents the index of the bolt-row, starting from the row furthest from the centre of compression, which is assumed to be aligned with the compressive beam flange for endplate connections;
- h_i is the distance of the ith bolt-row from the centre of compression;
- $k_{eff,i}$ is the effective stiffness coefficient for each bolt-row, given by Eq. (20):

$$k_{\text{eff},i} = \frac{1}{\frac{1}{k_{\text{rf}\,i}} + \frac{1}{k_{\text{rwT}\,i}} + \frac{1}{k_{\text{rn}\,i}} + \frac{1}{k_{\text{hT}\,i}}} \tag{20}$$

which is calculated based on the active components for that row, such as the column flange in bending $k_{\rm cf,i}$, column web in tension $k_{\rm cwT,i}$, endplate in bending $k_{\rm ep,i}$ and bolts in tension $k_{\rm bT,i}$.

The term $k_{\rm eq}$ in Eq. (18) represents the equivalent stiffness of the combined characteristics of all bolt rows, which is defined by the following expression:

$$k_{\rm eq} = \frac{\sum_{i} k_{\rm eff,i} h_i}{z_{\rm eq}} \tag{21}$$

In Eq. (18), $k_{\rm C}$ represents the stiffness coefficient of compression zone. For endplate connections, the compression stiffness of beam flange/web is assumed to be infinite, thus $k_{\rm C}$ is taken as the compression stiffness of column web $k_{\rm cwC}$, i.e. $k_{\rm C}=k_{\rm cwC}$. The term $k_{\rm V}$ represents the stiffness coefficient of shear zone, which is taken as the shear stiffness of column web panel $k_{\rm cwV}$, i.e. $k_{\rm V}=k_{\rm cwV}$. Further details on the calculation of the stiffness of each component can be found in EN 1993–1–8:2024

4.2. Plastic resistance

When calculating the design plastic resistance of the connection, the active components in tension zone are simplified by considering equivalent T-stubs for each bolt row, as shown in the inset in Fig. 12. The T-stubs are considered to fail in one of three modes [3]: (i) Mode 1, where complete yielding occurs with plastic hinge forming at the junction and near the bolts, (ii) Mode 3, where failure is due solely to bolt tension and (iii) Mode 2, which involves a combination of plastic hinge forming at the junction and bolt tension failure. Based on the development of a plastic mechanism, EN 1993–1–8:2024 [3] provides calculations to determine the strength of the T-stub for each failure mode, with the weakest of the three selected as the resistance of the equivalent T-stub.

As mentioned previously, the component-based design method as given in EN 1993–1–8:2024 [3] provides the equations for calculating the design plastic resistance of beam-column connections at ambient temperature. In the current study, these calculations are also adapted for

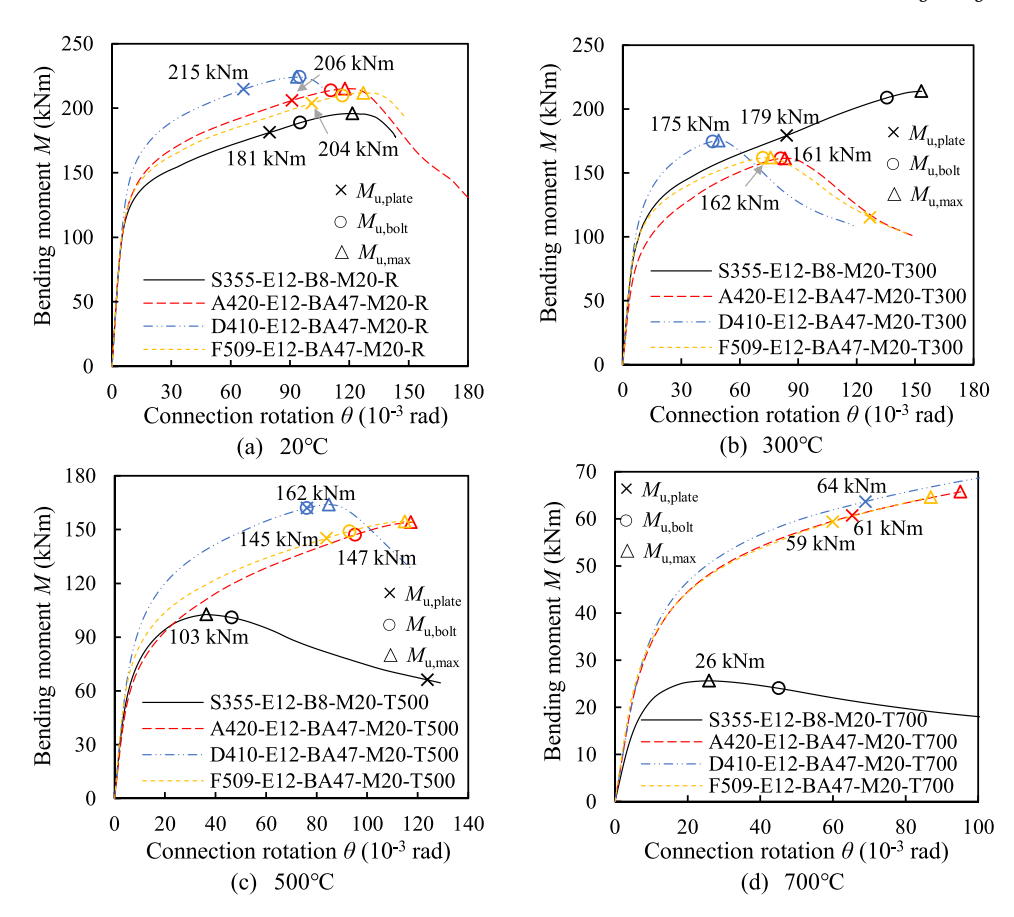


Fig. 10. $M-\theta$ curves of connections incorporating 12 mm thick endplates and M20 bolts made of various material grades at temperatures of (a) 20°C, (b) 300°C, (c) 500°C and (d) 700°C.

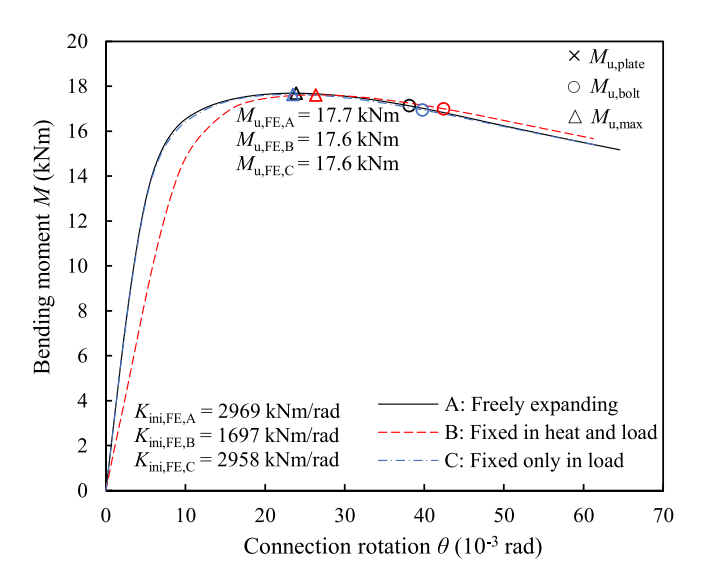


Fig. 11. M- θ curves for connection S355-E12-B8-M16-T700 with different boundary conditions at the top end of the column.

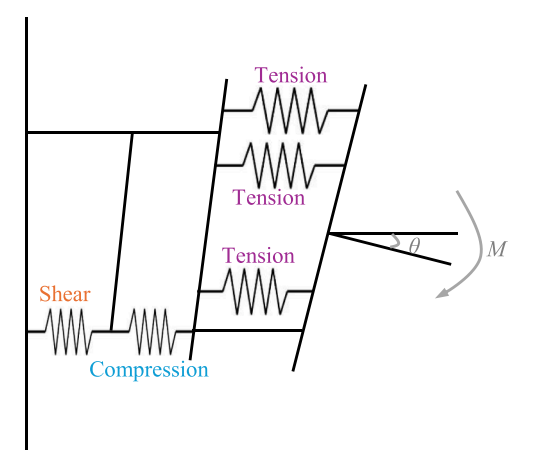
application in elevated temperature design. Hence, the design plastic resistance M_y of extended endplate beam-column connections is determined as:

$$M_{y} = \sum_{i} F_{i} h_{i} \tag{22}$$

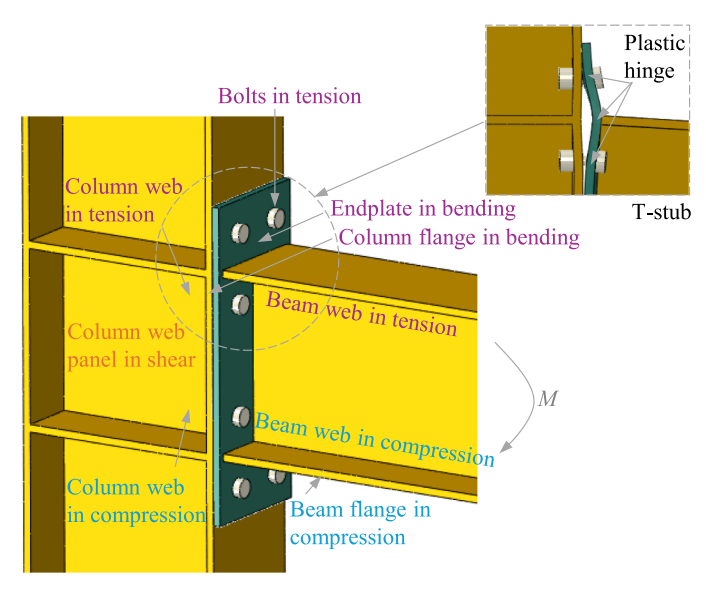
where F_i is the effective design tension resistance of the i^{th} bolt-row,

defined by the smallest component resistance within that bolt-row. For each bolt-row, the design tension resistance F_i should be calculated either: (i) individually for that bolt-row, or (ii) collectively for a group that includes that bolt-row and additional rows further away from the centre of compression; with the selection being defined by whichever outcome yields a more conservative result. For example, the tension resistance F_2 should be determined as the lower of the two values: (i) the tension resistance of Row 2 considered alone and (ii) the tension resistance of Row 1–2 group minus the tension resistance of Row 1 F_1 . The design tension resistance F_i should also be in equilibrium with the resistance of the compression zone. Thus, if the sum of the tensile resistance F_i exceeds the resistance of the compression zone, the effective tension resistance should be reduced, starting from lowest row and progressing upwards, until equilibrium is achieved.

To remain consistent with the provisions in the European structural steel fire design standard EN 1993-1-2:2024 [12], which specifies that the stress at 2 % total strain at elevated temperatures $f_{2,T}$ should be used as the reference material strength when determining the design cross-section resistance or member resistance of steel and stainless steel structures, in this study, $f_{2,T}$ is also recommended as the reference material strength for calculating the design resistance for each connection component. However, since a fire is typically considered to have an adverse effect on the structural resistance, it is recommended herein that the design resistance of components at elevated temperatures should not exceed their respective design resistance at room temperature. This is best exemplified by considering the design resistance of stainless steel components at elevated temperatures, where the reference material strength should be taken as $f_{2,T}$. However, this value should not exceed the 0.2 % proof stress at room temperature $f_{\rm p0.2}$, since $f_{\rm p0.2}$ is recommended as the reference material strength for room temperature design in prEN 1993-1-4 [26], which is the Eurocode standard for the design of



(a) Spring assembly



(b) Active components

Fig. 12. Spring assembly and active components of extended endplate beam-column connections.

structural stainless steel at room temperature.

4.3. Ultimate strength and deformation capacity

It can be observed from Figs. 6–10 that there may be considerable post-yielding stiffness and strength in connections. However, the component-based design method as currently implemented in EN 1993–1–8:2024 [3] only allows for the prediction of initial stiffness $K_{\rm ini}$ and plastic strength $M_{\rm y}$, without taking into account the ultimate strength $M_{\rm u}$. Therefore, in the current study, the four-parameter exponential model proposed by Yee [5] is extended to design of connections at elevated temperatures, as given in Eq. (23),

$$M = M_{y} \left\{ 1 - \exp\left[\frac{-\left(K_{\text{ini}} - K_{p} + c\theta\right)\theta}{M_{y}}\right] \right\} + K_{p}\theta$$
 (23)

which provides an approximation for the bending moment-rotation M- θ relationship. The M- θ curve derived through this expression satisfies the following four requirements: (i) the curve passes through the origin, i.e. M=0 at $\theta=0$; (ii) the slope of the curve at the origin is equal to the initial stiffness $K_{\rm ini}$, i.e. $dM/d\theta=K_{\rm ini}$ at $\theta=0$; (iii) when the rotation becomes large, the curve slope approaches the strain hardening stiffness of the connection, i.e. $dM/d\theta=K_{\rm p}$ as $\theta\to\infty$; (iv) for any rotation θ , the

slope of the curve corresponds to the tangent stiffness of the connection. This results in Eq. (23) being defined by parameters that are physically meaningful. The parameter c in Eq. (23) represents the shape parameter; it is seen to have a negligible influence on the response, and is taken as 0 for endplate connections as suggested in [5]. The strain hardening stiffness K_p is currently taken as 0.02 of initial stiffness K_{ini} , based on a reasonable fit to steel connection data obtained from [27]. Substituting these values into Eq. (23) yields:

$$M = M_{\rm y} \left\{ 1 - \exp\left[\frac{-0.98K_{\rm ini}\theta}{M_{\rm y}}\right] \right\} + 0.02K_{\rm ini}\theta \tag{24}$$

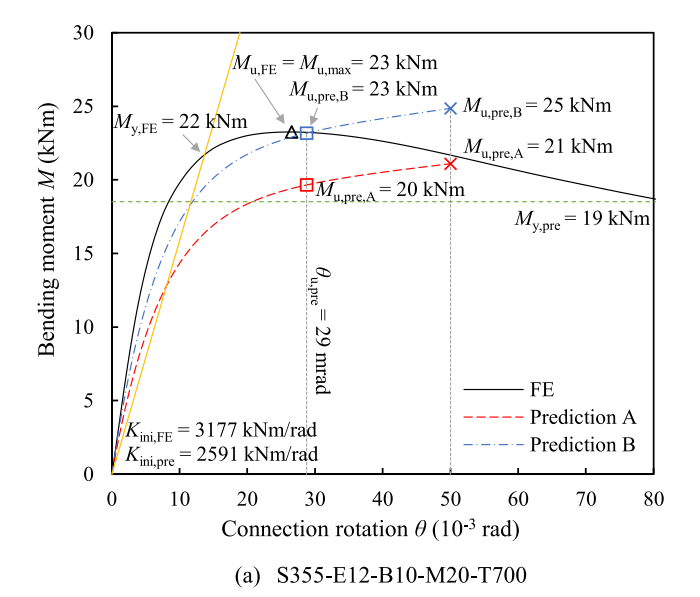
from which the moment-rotation curve $M-\theta$ can be estimated. However, owing to the exponential term in the expression, the response continues to increase without an upper limit. Considering that beam-column connections have finite rotation capacities, it is necessary to define a rotation limit at which the M- θ curve will be terminated to determine the ultimate connection strength. According to a study elsewhere [28], a connection can be considered sufficiently ductile if it achieves a rotation of 0.05 rad. This rotation limit was adopted in [29,30] to determine the design ultimate strength, with $M_{\rm u}$ defined as the bending moment at the rotation of 0.05 rad. However, this rotation limit was primarily derived based on room temperature case studies and may not be appropriate for elevated temperature design or for the design of hybrid connections. As shown in Figs. 6-10, the connection rotation at ultimate strength exceeds 0.05 rad for most connections at ambient temperature and 300°C. In contrast, at 500°C and 700°C, due to material degradation at elevated temperatures, the connection rotation at ultimate strength is lower than 0.05 rad in several cases – except for connections incorporating stainless steel components, which further highlights the advantages of hybrid connections. Therefore, to avoid potentially unsafe predictions of ultimate strength when using 0.05 rad as the rotation limit to terminate the $M-\theta$ curve derived from Eq. (24), an approach for determining the rotation limit θ_{ij} that accounts for the effects of various material grades and elevated temperatures is currently proposed:.

$$\theta_{\rm u} = 0.05 \, {\rm rad} \times \varepsilon_{{\rm u},T} / \varepsilon_{{\rm u,basic}} = 0.05 \, {\rm rad} \times k_{\varepsilon_{\rm u},T} \varepsilon_{\rm u} / \varepsilon_{{\rm u,basic}}$$
 (25)

In Eq. (25), $\varepsilon_{u,T}$ is the material strain at the ultimate stress of the critical element at temperature level T, which is calculated by multiplying the elevated temperature ductility reduction factor $k_{\varepsilon u,T}$ (see Section 2.1.2) by its room temperature strain ε_u . The term $\varepsilon_{u,basic}$ represents the material strain at the ultimate stress of the basic material grade at room temperature for the same element. The basic material grade is defined in the following manner: if the critical element is the bolt, the basic material grade is G8.8; if the critical element is the endplate or beam/column plates, the basic material grade is S355. This implies that for a connection comprising G8.8 bolts, S355 endplate and S355 beams and columns, the rotation limit for determining its ultimate resistance at room temperature is set at 0.05 rad. In considering this as a baseline, the effects of different material grades are accounted for through the ratio of $\epsilon_{\text{u}}/\epsilon_{\text{u,basic}}$, while the influence of ductility degradation at elevated temperatures is incorporated through the reduction factor $k_{e_{\parallel},T}$. Based on this proposed rotation limit θ_{\parallel} , the design ultimate strength of the connection is determined as the bending moment at the point on the M- θ curve which terminates at the connection rotation $\theta_{\rm II}$. In the currently proposed method, the governing component for the plastic connection resistance M_y , calculated through the component-based method from EN 1993-1-8:2024 [3], is considered to be the governing component at M_{II} . However, a component (such as a T-stub) may be formed of several elements, and since the limit θ_{ij} is defined using strain limits it would be prudent to identify which element within the component has failed. Therefore, it is currently considered that if the governing component is the endplate T-stub or column flange T-stub: for failure mode 1 the endplate or column flange is considered to be the critical element, whereas for failure modes 2 and 3 the bolt is regarded as the critical element. The proposed recommendations for the rotation limit are recommended on the basis of a preliminary study, and hence a more comprehensive investigation is warranted for further improvement in future research.

5. Application of the proposed design method

The current section demonstrates the application of the proposed design methods through two examples, S355-E12-B10-M20-T700 and A420-E12-BA47-M20-T700, which are presented in Fig. 13. The predicted initial stiffness $K_{\rm ini,pre}$ and plastic strength $M_{\rm y,pre}$ are calculated using Eqs. (18) and (22), respectively. The numerical initial stiffness $K_{\rm ini,FE}$ and plastic strength $M_{\rm y,FE}$ obtained from the FE models are also presented in Fig. 13. According to EN 1993–1–8 [3], the numerical plastic strength $M_{\rm y,FE}$ is determined by the intersection of the M- θ curve and a secant line with a slope of $K_{\rm ini,FE}/\eta$, where the modification coefficient η is taken as 2 for endplate connections. As shown in Fig. 13, for these two connections, the plastic strengths predicted by the component-based design method $M_{\rm y,pre}$ are very similar to the corresponding FE value $M_{\rm y,FE}$. However, the predicted initial stiffnesses $K_{\rm ini,pre}$ are conservative when compared with the numerical values $K_{\rm ini,FE}$, with a difference of



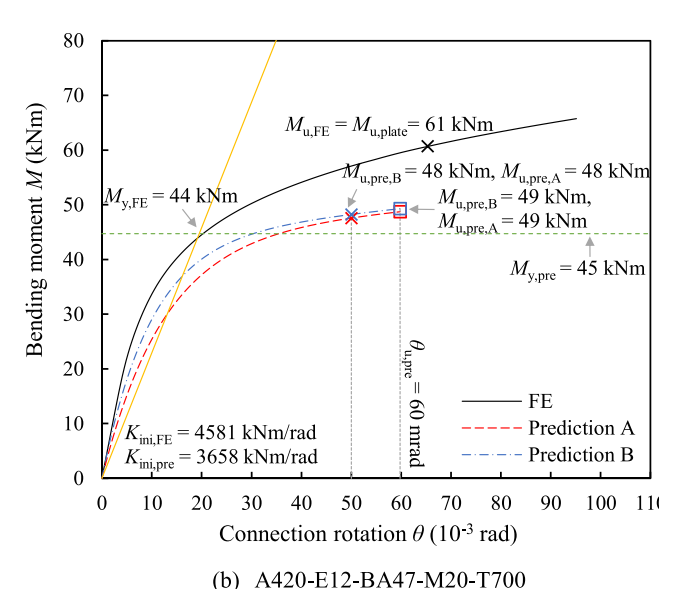


Fig. 13. Application of developed fire design method for beam-column connections.

Table 8Summary of comparison of predicted initial stiffness, plastic resistance and ultimate resistance against benchmark FE results for all studied connections.

$K_{\rm ini,pre}/K_{\rm ini,FE}$	$M_{\rm y,pre}/M_{\rm y,FE}$	$M_{ m u,pre}/M_{ m u,FE}$
0.84	0.93	0.77
0.064	0.090	0.074
0.96	1.09	0.88
0.70	0.76	0.60
	0.84 0.064 0.96	0.84 0.93 0.064 0.090 0.96 1.09

approximately 20 % noted in both cases. In addition to the FE $M-\theta$ curve. an additional two $M-\theta$ curves are shown in the Fig. 13, which are labelled as Predictions A and B respectively. Prediction A represents the $M-\theta$ curve determined using Eq. (24) using the assumed initial stiffness $K_{\rm ini,pre}$ and plastic strength $M_{\rm v,pre}$, whereas in Prediction B the numerical values obtained from FE models $K_{\text{ini,FE}}$ and $M_{\text{v,FE}}$ are substituted into Eq. (24). The rotation limit baseline of 0.05 rad as well as $\theta_{u,pre}$ calculated using the proposed Eq. (25) are also shown in the figure. As observed in Figs. 6-10 and discussed in Section 4.3, at higher elevated temperatures, e.g. at 500°C and 700°C, the connection rotation at the ultimate strength falls below 0.05 rad in several cases, indicating that using 0.05 rad as the rotation limit for determining the design ultimate strength may be inappropriate. From Fig. 13 (a), it is observed that the rotation limit proposed in this study $\theta_{u,pre}$, which is equal to 0.029 rad for the currently considered case, effectively accounts for the reduction in rotation at elevated temperatures, whereas a rotation limit of 0.05 rad leads to an unsafe prediction thereby demonstrating its unsuitability. On the other hand, owing to the superior ductility of stainless steel at elevated temperatures, the connection rotation at the ultimate strength can exceed 0.05 rad as shown in Fig. 13 (b). For this case, the proposed rotation limit $\theta_{u,pre}$ is calculated to be 0.060 rad, demonstrating the capability to effectively capture the effect of using different material grades. Furthermore, when applying the same rotation limit $\theta_{u,pre}$, the ultimate strength prediction based on the $M-\theta$ curve given by Prediction B $M_{\rm u,pre,B}$ is more accurate than the corresponding value from Prediction A, $M_{\rm u,pre,A}$. This indicates that the conservatism in the ultimate strength predictions is partly due to the conservative values for initial stiffness and plastic strength used in their determination.

The initial stiffness, plastic strength and ultimate strength predicted using the proposed design method and the benchmark FE results for studied connections at different temperature levels are listed in Tables 4–7. The ratios of predictions to FE results, i.e. $K_{\rm ini,pre}/K_{\rm ini,FE}$, $M_{\rm y,pre}/M_{\rm y,FE}$ and $M_{\rm u,pre}/M_{\rm u,FE}$, are also included in the tables. The mean, coefficient of variation (CoV), maximum and minimum values of these three ratios for all studied connections are summarised in Table 8. The predicted plastic strengths $M_{\rm y,pre}$ of connections are shown to be generally accurate and safe, whereas the predicted initial stiffnesses $K_{\rm ini,pre}$ and ultimate strengths $M_{\rm u,pre}$ tend to be slightly conservative. It is worth noting that if the numerical values of initial stiffness and plastic strength are substituted into Eq. (24), instead of the predicted values using Eqs. (18) and (22), the conservatism in the ultimate strength predictions could be reduced.

6. Conclusions

The current paper investigates the behaviour of steel and hybrid extended endplate beam-column connections at ambient and elevated temperatures though numerical analysis. Following validation against experimental results, the developed FE models are utilised to conduct extensive parametric studies, considering the influence of various endplate thicknesses and material grades, bolt sizes and material grades, and temperature levels. The results obtained from the numerical analysis indicate that replacing carbon steel components with stainless steel components in critical areas of connections, such as endplates and/or bolts, leads to improvements in strength and rotation capacity, especially at higher elevated temperatures (e.g. 500°C and 700°C), which are

critical in steel framed structures. In this study, the component-based design method given in EN 1993–1–8:2024 [3] is extended to address fire scenarios, allowing the determination of design initial stiffness and plastic strength for connections at elevated temperatures. Additionally, an alternative design approach for predicting the ultimate strength of connections is presented, along with a new methodology for determining the rotation limit. Compared with the benchmark FE results, the predictions for initial stiffness, plastic strength and ultimate strength of steel and hybrid beam-column connections are shown to be accurate and safe in general, however, determining a more appropriate rotation limit remains a topic for future research.

CRediT authorship contribution statement

Chunyan Quan: Writing – original draft, Visualization, Validation, Software, Methodology, Investigation, Formal analysis, Data curation, Conceptualization. Luke Lapira: Writing – original draft, Supervision, Software, Methodology, Investigation, Conceptualization. Katherine Ann Cashell: Writing – review & editing, Supervision, Project administration, Methodology, Investigation, Funding acquisition, Conceptualization.

Declaration of Competing Interest

The authors declare that there is no conflict of interest.

Acknowledgements

This research is funded by the Engineering and Physical Sciences Research Council (EPSRC) [EP/W019809/1]. The authors gratefully acknowledge the financial support of the EPSRC.

Data availability

Data will be made available on request.

References

- Gao JD, Yuan HX, Du XX, Hu XB, Theofanous M. Structural behaviour of stainless steel double extended end-plate beam-to-column joints under monotonic loading. Thin Walled Struct 2020;151:106743.
- [2] Gardner L. Stainless steel structures in fire. Proc Inst Civ Eng Struct Build 2007; 160:129–38.
- [3] EN 1993-1-8:2024. Eurocode 3: Design of steel structures Part 1-8: Joints. 2024.
- [4] Zhu C, Rasmussen KJR, Yan S. Generalised Component Model for Structural Steel Joints. J Constr Steel Res 2019;153:330–42.
- [5] Yee Y, Melchers R. Moment-rotation curves for bolted connections. J Struct Eng ASCE 1986;112(3):615–35.
- [6] ABAQUS. ABAQUS/Standard User's Manual. Version 6.17. Dassault Systemes Simulia Corp. USA; 2017.

- [7] Qiang X, Wu N, Jiang X, Luo Y, Bijlaard F. Experimental and numerical analysis on full high strength steel extended endplate connections in fire. Int J Steel Struct 2018;18:1350–62.
- [8] Lu P, Yang J, Ran T, Wang W. Experimental study on flexural capacity and fire resistance of high strength Q690 steel flush end-plate connections. ThinWalled Struct 2023;184:110506.
- [9] Qiang X, Wu N, Luo Y, Jiang X, Bijlaard F. Experimental and theoretical study on high strength steel extended endplate connections after fire. Int J Steel Struct 2018; 18:609–34.
- [10] BS EN ISO 3506-1:2020, Fasteners Mechanical properties of corrosion-resistant stainless steel fasteners, Part 1: Bolts, screws and studs with specified grades and property classes. 2020.
- [11] Song Y, Wang J, Uy B, Li D. Experimental behaviour and fracture prediction of austenitic stainless steel bolts under combined tension and shear. J Constr Steel Res 2020;166:105916.
- [12] EN 1993-1-2:2024. Eurocode 3: Design of steel structures Part 1-2: General rules – Structural fire design. 2024.
- [13] Quan C, Kucukler M. Design of stainless steel SHS and RHS columns in fire by GMNIA with strain limits. Eng Struct 2024;316:118464.
- [14] Ban H, Yang Q, Shi Y, Luo Z. Constitutive model of high-performance bolts at elevated temperatures. Eng Struct 2021;233:111889.
- [15] Design Manual for Structural Stainless Steel, fourth ed., Steel Construction Institute (SCI), 2017..
- [16] Fang H, Chan TM. Resistance of axially loaded hot-finished S460 and S690 steel square hollow stub columns at elevated temperatures. Structures 2019;17:66–73.
- [17] Li D, Uy B, Wang J, Song Y. Behaviour and design of Grade 10.9 high-strength bolts under combined actions. Steel Compos Struct 2020;35:327–41.
- [18] Ling Y. Uniaxial true stress-strain after necking. AMP J Technol 1996;5(1):37-48.
- [19] Coelho AMG. Characterization of the Ductility of Bolted Endplate Beam-to-Column Steel Connections (PhD thesis). Universidade de Coimbra; 2004.
- [20] Pang XP, Hu Y, Tang SL, Xiang Z, Wu G, Xu T, Wang XQ. Physical properties of high-strength bolt materials at elevated temperatures. Results Phys 2019;13: 102156.
- [21] Huang L, Li GQ, Wang XX, Zhang C, Choe L, Engelhardt M. High Temperature Mechanical Properties of High Strength Structural Steels Q550, Q690 and Q890. Fire Technol 2018;54:1609–28.
- [22] Liang Y, Manninen T, Zhao O, Walport F, Gardner L. Elevated temperature material properties of a new high-chromium austenitic stainless steel. J Constr Steel Res 2019;152:261–73.
- [23] C. Quan M. Kucukler Elevated temperature material behaviour and testing of novel, cost-efficient and high-performance stainless steel grades Thin-Walled Struct. (accepted).
- [24] Manninen T, Säynäjäkangas J. Mechanical Properties of Ferritic Stainless Steels at Elevated Temperature. Proc Fourth Int Expert Semin Stainl Steel Struct 4th 2012: 1–15.
- [25] Hu Y, Yang CB, Teh LH, Yang YBin. Reduction factors for stainless steel bolts at elevated temperatures. J Constr Steel Res 2018:148:198–205.
- [26] prEN 1993-1-4. Eurocode 3: Design of steel structures Part 1-4: General rules -Supplementary rules for stainless steels. 2021.
- [27] Jing Q. Study on M- θ Relationships of Extended End Plate Connection of Steel Frame. Shanghai: Tongji University; 2004 (in Chinese).
- [28] Sun FF, Sun M, Li GQ, et al. Experimental study on seismic behavior of high strength steel beam-to-column end-plate connections. J Build Struct 2014;35(4): 116–24.
- [29] Chen Z, Wang W, Wang Z. Experimental study on high-strength Q460 steel extended end-plate connections at elevated temperatures. J Constr Steel Res 2023; 200:107686.
- [30] Wang W, Qian Z, Zhang Y, Wang Z. Experimental and numerical study on behaviour of extended end-plate connections with Q960 steel at elevated temperature. J Constr Steel Res 2024;213:108384.